Clean Technologies and Recycling

http://www.aimspress.com/journal/ctr

Clean Technologies and Recycling, 2(1): 32–46.
DOI: 10.3934/ctr.2022002
Received: 10 November 2021
Revised: 23 January 2022
Accepted: 10 February 2022
Published: 23 February 2022

Research article

Characterization of recycled Inconel 718 metal powder for assessing its reusability in the laser powder bed fusion process

Susana J. Castillo[1], Anna Hayes[1], Greg Colvin[2], Barrett G. Potter[1,3], Rongguang Liang[3] and Krishna Muralidharan[1,4,*]

[1] Department of Materials Science and Engineering, University of Arizona, Tucson, AZ 85721, USA
[2] Honeywell Aerospace, Phoenix, AZ 85721, USA
[3] College of Optical Sciences, University of Arizona, Tucson, AZ 85721, USA
[4] Lunar and Planetary Laboratory, University of Arizona, Tucson, AZ 85721, USA

* **Correspondence:** Email: krishna@email.arizona.edu; Tel: +15206268997.

Abstract: Additive manufacturing technologies such as laser powder bed fusion (LPBF) provide unprecedented abilities to manufacture complex 3-D parts and structures; however, the process produces leftover metal powder that is often unused, resulting in significant cost and disposal overhead. Towards this end, to ensure the ability to recycle the unused powder that is typically found within the build volume and in the overflow compartments of LPBF systems, a thorough chemical and structural analysis is required. Such an analysis will help in determining the extent of recyclability and reusability of the unused powder. For these purposes, characterization of recycled powder for Inconel 718 was performed in this work as a function of build-cycle to compare and contrast the evolution in physical and chemical properties such as particle size distribution, morphology, and composition. We note that the analysis was carried out for 21 build-cycles. Characterization of the particle size distribution and circularity was performed using traditional scanning electron microscopy methods and that information was later compared to measurements of surface profile using coherent scanning interferometry. Reusability was assessed using these results in conjunction with chemical analysis of the powder that was carried out using energy dispersive X-ray spectroscopy. For the extent of build-cycles considered in this work, it was seen that the physical and chemical changes in the recycled powder were will within accepted limits for powder usage and that with appropriate measures, recycled powder can be re-incorporated for subsequent builds without compromise in the powder quality. This study provides a pathway for greatly reducing powder consumption and thus cost during the LPBF process.

Keywords: additive manufacturing; recycled powder; particle size distribution; coherent scanning interferometry; circularity; mechanical properties; porosity

1. Introduction

Laser powder bed fusion (LPBF) based additive manufacturing (AM) methods provide the ability for on-demand production of specialized engineering parts and devices with complex structural topologies that otherwise cannot be fabricated using conventional methods. Such capabilities dramatically impact the design of metallic parts and components especially for aerospace, automobile, defense and medical applications [1].

For fabrication of metal parts and components, LPBF offers certain advantages over other competing technologies. In particular LPBF provides better resolution, lower energy consumption and higher density parts [2]. It is applicable to any material that is weldable and can be produced in powder form; further, the powder bed offers support to the object being manufactured, and in general, the manufactured part does not require extensive post-treatment as compared to competing methodologies.

However, as with every metal-AM technology currently in use, LPBF still has disadvantages. The challenges include: (i) wide variations in part properties from build to build, (ii) need for several iterations to hit target requirements, (iii) residual stress created in the parts due to thermal gradients inherent to the process that can make a build fail while affecting the machine/system, and of particular relevance to this work—(iv) the cost associated with excess unused powder produced during the build-process.

In this regard, there has been multiple efforts focused on the ability to recycle and reuse the excess powder in subsequent builds [3–14]. However, there are knowledge-gaps in terms of obtaining a systematic build-cycle dependent evolution of physical and chemical characteristics of the excess powder produced during each build, and towards this end, we focus on characterizing the physical-chemical properties of excess powder as a function of build-cycle. In particular, we focus on systematically characterizing the build-cycle dependent evolution of the underlying particle size distribution (PSD), shape and morphology of the powder particles (i.e. deviations from the assumed spherical shape), and the chemical composition of the particles. The above characteristics are particularly relevant in determining the ability for reusing powder that remain unutilized during previous builds. In this regard, in this work, methods such as scanning electron microscopy, energy dispersive X-ray spectroscopy, coherence scanning interferometry were used for examining the powder characteristics.

Inconel 718 is chosen as the primary material to be studied in this work. This choice is driven by already available literature on AM processing of Inconel 718 [15] providing a ready baseline for initial validation. Further, Inconel 718 is very amenable to LPBF due to its weldability and is a high-strength, high-temperature superalloy finding immense aerospace applications.

2. Background

Metal and metallic alloys are one of the most widely used material-feedstocks for engineering applications; recent advances in alloy design [16] and topology optimization [17] have now provided the chance to tailor the design of metal parts for on-demand and targeted applications. Thus, parts with targeted properties such as hardness, fatigue strength, malleability, ductility, corrosion resistance, etc. can now be designed using AM that would not have been previously possible.

LPBF, also known as selective laser melting (SLM) or direct metal laser melting (DMLM), is widely adopted in the aerospace and automotive industries to manufacture metal parts.

The LPBF manufacturing approach involves many inter-dependent steps starting from the design to selection of feedstock material, to optimization of process parameters and post processing. Many studies have examined the interplay between the process and design parameters and their individual and collective roles on the build quality [18–23].

The design parameters for LPBF include: support structures design, topology optimization, distortion compensation, shrinkage compensation, tessellation accuracy and support structure design. The process parameters include: hatch spacing, scan velocity, laser power, laser spot size (beam diameter and shape), layer thickness, scanning strategy, number of lasers, gas flow direction and speed, type of gas, build plate material vs. build material, preheat or additional heating methods (of either build plate, build volume walls, top surface using resistive heaters, additional radiative heat, heat from prolonged laser radiation), cooling methods, other environmental parameters, recoater blade speed, and dose factor. Some of these process parameters are directly related to the material properties while others may still be indirectly dependent on them. Further, there are post processing steps needed once the initial build is performed; these steps include: removal from build plate process, support removal, trapped powder removal, shot peening, heat treatment, hot isostatic pressing, surface finishing, and cosmetic coatings.

The focus of this work resides in how feedstock powder can be recycled and how powder characteristics evolve with reuse. This requires the accurate identification of its interplay with the various process and design parameters. For these purposes, this work will focus on evaluating the evolution in the integrity of the powder used in printing as a function of the number of ‘build-cycles’ to which it has been subjected, to compare and determine if recycling of used powder is viable for use in LPBF builds. Such a study would enable the optimization of recycling unused powder thereby ensuring significant cost-savings.

Powder reuse studies in LPBF manufacturing systems have been performed for most of the commonly used alloys in the industry. The results vary greatly depending on the alloy studied and on the parameters used during the process. This shows the necessity for specific experiments tailored to each system. In a study by Slotwinski et al. [4], 17-4 stainless steel and Cobalt chrome (CoCr) powder were characterized in their virgin state and later after different cycles to analyze changes in physical and chemical properties. Agglomerates formed in the AM process were hypothesized to be scraped away by the spreader or trapped when going through the sieve process but in general, the particles could not be fully removed from the powder. The 17-4 SS and CoCr powder feedstocks were analyzed by X-ray photo spectroscopy (XPS) showing no significant difference in the elemental composition of the powder from 8 cycles.

In another related study [5], the authors studied the powder from four different alloys, Inconel 718, Ti6Al4V, AlSi10Mg and Scalmalloy, to find that the powder characteristics studied showed a different severity in changes depending on the alloy. More lightweight alloys were concluded to be more affected by reuse and some aluminum alloys are more susceptible to a rise in oxygen content than alloys such as Ti6Al4V or Inconel 718.

Of particular relevance to this study is the work of Ardila et al. [6]; in this work they focused exclusively on Inconel 718 and reused feedstock powder up to 14 times to examine the role of recycling on the built parts. When comparing the properties of the powder in its initial or virgin state to the powder from 14 iterations, they found a change in the particle size distribution (~10%), which was attributed to the surge of particle aggregates during manufacturing. The chemistry analysis of the powder from the first and last cycles revealed virtually no change. When testing the metallurgical and mechanical aspects of the final built parts, they found that the porosity variation in the different build iterations was minimal (~0.1%). The authors further concluded by noting a material use efficiency of over 95%, with the remaining 5 % attributed to loss during the sieving process.

Other significant investigations include that of Gruber et al. [12], Paccou et al. [13], and Sendino et al. [14]. Specifically, Gruber et al. studied the physico-chemical evolution, morphology, and flowability of recycled Inconel 718 powder and noted that only spatter powder demonstrated degradation indicating the ability to use recycled powder without loss in performance. Similarly, Paccou et al also noted the lack of degradation in recycled powder in their work, where they compared parts manufactured from virgin powder and powder obtained after 50 cycles. They concluded that the respective microstructures and mechanical properties of Inconel 718 parts whether printed from virgin or recycled powder were very similar. In the work of Sendion et al, they showed that with increasing cycling, the morphology of the recycled particles changes with more satelliting and irregularities in their morphologies.

In a publication from Honeywell Aerospace [3], Inconel 718 powder was submitted to 10 build-cycles to study chemistry, particle size distribution and mechanical properties of the powder and parts from each cycle. Their investigation was inspired by a realization that, depending on the part they were manufacturing, only about 3–5% of the powder introduced into the LPBF system was actually melted to comprise the final built part. In terms of cost, that means that the price of the powder goes from a purchase price of $90/kg to an estimated cost of $3000/kg. Other than a small but gradual increase in oxygen content of the powder as a function of cycle, no significant changes were noticed in the powder characteristics or in the mechanical properties of the built parts.

Using the above studies as steppingstones, we extend the analysis of the interplay between build cycle and the evolution of powder characteristics, by focusing on a step-by-step evaluation of evolution with build-cycle (up to 21 cycles). We evaluate the evolution in morphology of the recycled powder in terms of their circularity in addition to particle size distribution. As a complement to traditional scanning electron microscopy (SEM) based methods, we also implement coherence scanning interferometry (CSI) for analyzing particle size distribution and circularity evolution. CSI has been employed in AM for surface texture measurements of as-manufactured and post-processed parts [24,25] and for in situ measurement of surface roughness of parts [26]. However, CSI has not been implemented for analysis of particle size and morphology and provides a rapid alternative to SEM, especially since there is no prior need for sample preparation in addition to its ability to being integrated inline during the LPBF process. Further, we use energy dispersive X-ray spectroscopy (EDS) to examine the chemical evolution and examine their combined effect on LPBF builds of sample specimens.

To supplement the findings on the particle evolution interplay with recycling, we also briefly report on the respective mechanical properties and porosities of targeted parts corresponding to different build-cycles, to discern possible effects of particle evolution on ensuing LPBF-built parts. However, we do note that a more detailed examination on the interplay between porosity, mechanical properties, and build-cycle will be reported in a follow-up paper, as the primary focus of this work is on characterizing the morphological and chemical evolution of recycled powder used in LPBF. Specifically, this work will provide guidelines to understand how many reuses a powder can withstand in general, giving the users a standardization guideline for knowing whether or not it is safe to reuse each material without compromising quality.

3. Experimental methods

The recycled powder analyzed in this work consists of unmelted and unutilized Inconel 718 powder in the build chamber and in the overflow compartments of an EOS M280 machine. At the end of every build-cycle, the collected powder is post-processed initially to eliminate spatter, agglomerated and oxidized particles created during the process. The recycled powder is also stirred to eliminate size segregation that naturally occurs. The base material was supplied by Praxair, the alloy brand name being TruForm 718 which is a powder form of the alloy Inconel 718 amenable for additive manufacturing processes. All specimen fabrication was done in the above EOS machine using optimized process parameters and post-processing as determined by the OEM [27], and the primary printed parts consisted of tensile test specimen bars of 0.5 inch diameter and varied between 6–12 inches in length. The samples were then analyzed for porosity and mechanical properties.

A total of 250 kg of virgin powder was used for the recycling study. The remaining unused powder after every build was used for the subsequent build and this cycle was repeated for a total of 21 build-cycles. A thorough analysis of the powder before and after every build iteration showed that about 0.8% of the weight of the powder was lost and unaccounted for, which was attributed to loss during transfer as well as powder trapped in the filters (i.e. dust on the internal surfaces of the chamber).

We also note that after every build, the remaining unmelted powder in the build volume and in the overflow compartments was sieved through a 53-micron sieve. The powder that was trapped in the sieve was removed and stored as waste. The sieved powder (that did pass through the sieve) was reused for successive builds. The recycled powder was also stirred to eliminate size segregation that naturally occurs. While the diameter of the printed samples was always 0.5 inch in diameter, the lengths of the parts printed varied with each successive build due to the fact that each iteration had less total powder to work with and thus the specimen lengths ranged from 12 inches (1–12 build cycles) to 6 inches (13–21 build cycles). In this regard, to ensure consistency in reporting the mechanical properties and porosities of built-parts, we only focus on the samples with lengths equaling 12 inches.

For effective characterization, after every build and prior to sieving, samples of powder were taken from different areas of the build volume to sample used powder that had been affected in variety of ways such as powder from initial layers that remained in the build volume for longer or shorter times as well as powder that was closer or farther away from the heat affected zone (HAZ).

The sieved powder samples were used for analysis corresponding to particle size distribution, morphology, and chemistry, while the built samples were tested for internal cracks and defects using nondestructive evaluation nonlinear ultrasonics.

The particles were analyzed using three characterization methods: scanning electron microscopy (SEM), energy dispersive X-ray spectroscopy (EDS), and coherence scanning interferometry (CSI).

Test specimens were printed on the above-mentioned EOS M 290 LPBF system using default machine parameters for Inconel 718. Cross-sections of built samples of gauge-length equaling 12.5 mm were prepared using a standard metallographic grinding and polishing procedure for porosity evaluation. A Keyence optical microscope was used to image the samples and the provided image analysis software was used for evaluating the porosity of the different samples. Porosity was measured at five different heights for each of the samples under consideration and the average values were reported.

An MTS mechanical tester was used for obtaining mechanical properties such as yield strength (YS), and ultimate tensile strength (UTS) of select samples. Three samples for each build-cycle were used for determining the mechanical properties providing appropriate statistical bounds.

The SEM machine used was a Hitachi desktop SEM TM4000 Plus. Samples were mounted on 6 mm aluminum stubs using adhesive carbon tape. Powder was scooped using a spatula and sprinkled on the adhesive to obtain a sample where the particles are spaced on the carbon tape making it easier to discern them individually in the images. The SEM accelerating voltage was 15 kV, and the BSE detector was set to a magnification of 300×. Low brightness and high contrast were used to clearly define the metal powder particles from the carbon tape.

The CSI instrument used for particle size analysis was a Zygo Nexview Optical Profiler which uses its own proprietary software. Depending on the sample, the focus, intensity, scan length and scanning speed on the interferometer were appropriately adjusted. Powder samples were prepared for analysis using a doctor blade to spread a uniform layer of metal powder with layer thickness of 40μm over an SEM sample holder.

In order to evaluate how the chemistry of the powder changes, energy dispersive X-ray spectroscopy was performed on representative samples using a Bruker Quantax 70 Energy Dispersive X-ray Spectrophotometers coupled to a Hitachi TM3000 TableTop SEM. The samples used were the same used for the SEM analysis.

4. Results and discussion

As a first step towards obtaining the evolution of the powder characteristics, we present particle size distribution (PSD) as a function of build-cycle as calculated from SEM data. Specifically, in Figure 1 we present the PSD for the following samples: virgin, 1 cycle, 5 cycles, 9 cycles, 13 cycles, 17 cycles, and 21 cycles. As seen in Figure 1, the PSD variation is minimal with with increasing number of builds, though there is a slight skew towards larger PSD for higher build-cycles. The slight shift towards higher PSD for higher build-cycles is clearly illustrated in a comparison of the PSD for virgin vs. PSD for the 21st build-cycle (Figure 2). Of note is the loss of "fines" in the PSD of the 21st build cycle (attributed to repeated sieving between each cycle), while the increase in the number count of larger particles is attributed to possible formation of larger agglomerates during each build cycle.

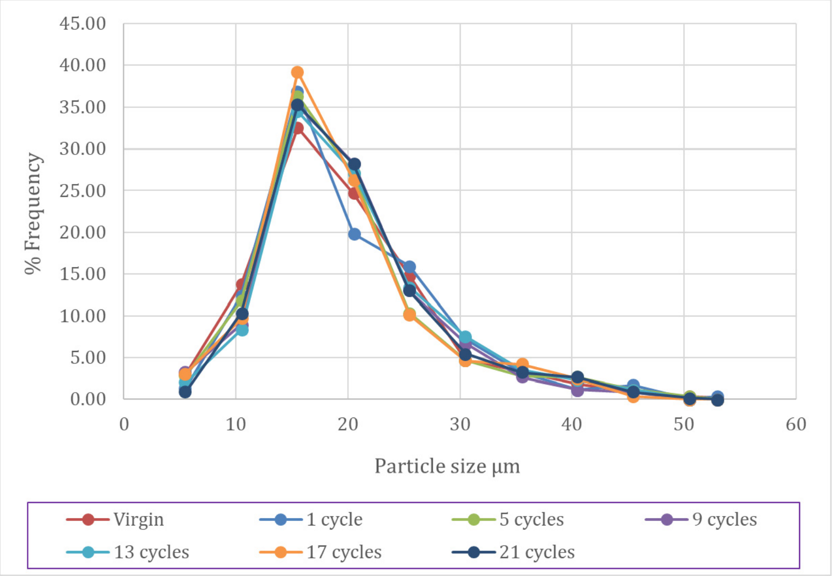

Figure 1. Particle size distribution evolution as a function of build-cycle.

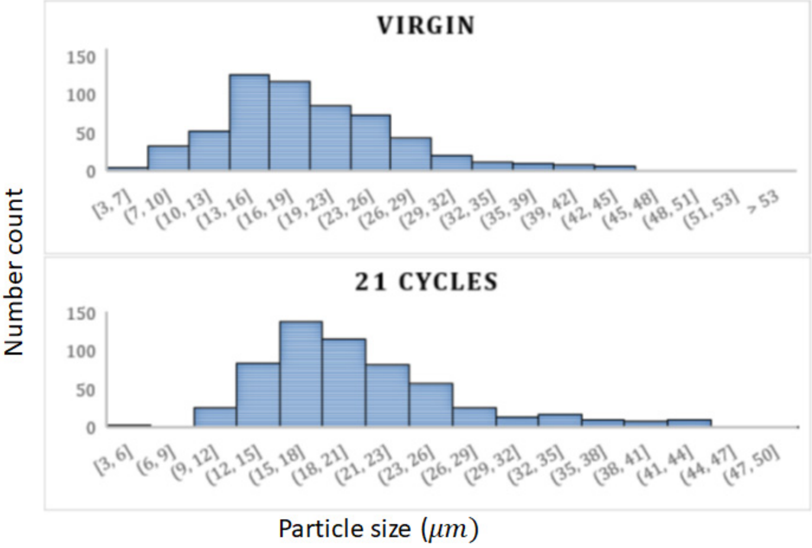

Figure 2. Particle size distribution comparison between virgin powder and recycled powder obtained after 21 build-cycles.

More importantly, there is no systematic variation in the measured D50 value and essentially the D50 value remains uniform as a function of build cycle (as reported in Table 1). Here the D50 value denotes the median particle size where 50% of the particle sizes are larger and 50% smaller. On this note, a comparison between virgin versus recycled powder after 21 cycles shows that the D10 values of powder corresponding to virgin vs that obtained after 21 cycles were 12.02 μm and 14.30 μm respectively, while the corresponding D90 values were 30.67 μm vs 31.32 μm respectively. While these trends are consistent with past investigations [3,5,6,12], it needs to be pointed out that none of the previous studies did an elaborate sampling of PSD dependence on the number of cycles as compared to this work.

Table 1. D50 values (in μm) for the cycled powder.

	Virgin	1 cycle	5 cycles	9 cycles	13 cycles	17 cycles	21 cycles
D50	18.56	18.14	17.69	18.45	19.15	17.68	18.69

We note that for the purposes of obtaining the respective PSDs, we analyzed a total of 10 SEM images per sample, which corresponded to upwards of 600 particles for each sample. A representative SEM image is shown in Figure 3, corresponding to the virgin sample.

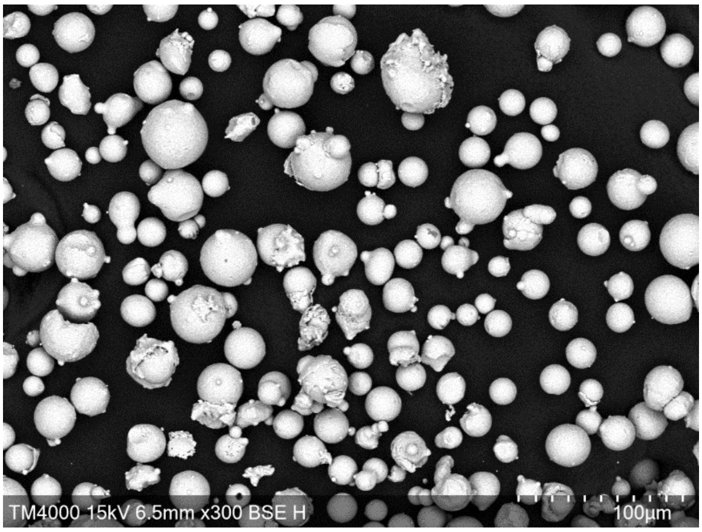

Figure 3. An illustrative SEM image of the virgin sample.

For calculating the PSD, the ImageJ software with Fiji plugins was utilized; The software was used to make a projected image of the particles, from which their diameter (and circularity- discussed in a subsequent subsection) were calculated. Specifically, each SEM image was processed such that the hue, saturation, and brightness were adjusted for every image until all the particles were color-filled completely while the background was unfilled. Next all colored pixels were converted into white with a value of 1, and all uncolored pixels were converted to black with a value of 0. The image was then subjected to a watershed filter to clearly distinguish each particle, even when particles touch each other; from these images the perimeter, diameter and circularity were obtained using ImageJ. Each particle outline was numbered for individual traceability in the data file. The process described is illustrated in Figure 4.

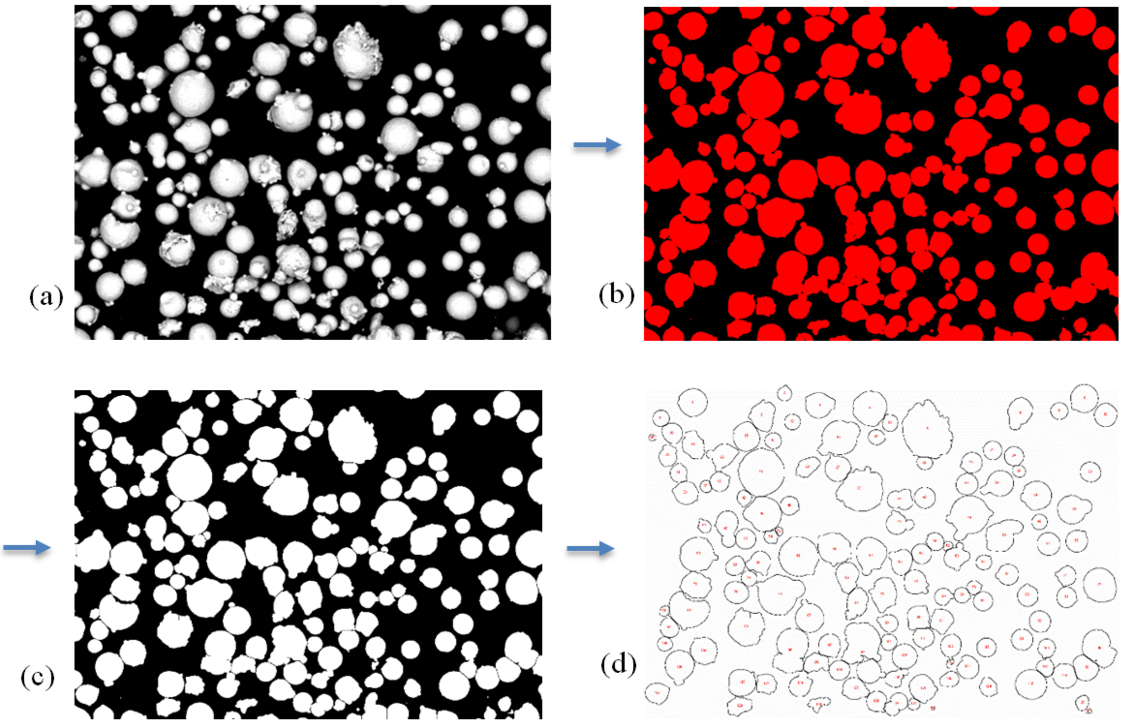

Figure 4. Analysis of an SEM image using (a) smoothing filters; (b) color threshold; (c) binary and watershed; in (d) outlines of analyzed particles is provided.

As a complement to SEM as well as an orthogonal verification tool, we also used CSI to calculate PSD as a function of build-cycle. Compared to SEM, CSI represents a more versatile tool, capable of large-area imaging, real-time analysis as well as the ability to get a depth profile simultaneously. In this work, the PSD evolution as obtained from CSI was very similar to SEM results, underlining the accuracy of our analysis. The typical difference in estimation between SEM and CSI was ±5 µm and the method used for estimating PSD from CSI is further elaborated below.

Figure 5 represents a CSI-derived image of the virgin powder layer. In Figure 5, a color pallet to visualize the powder layer topography/elevation is provided; the average height (arithmetic mean) is in green, the lowest points are in blue, the highest points are in red, and a corresponding color progression is applied for values in between.

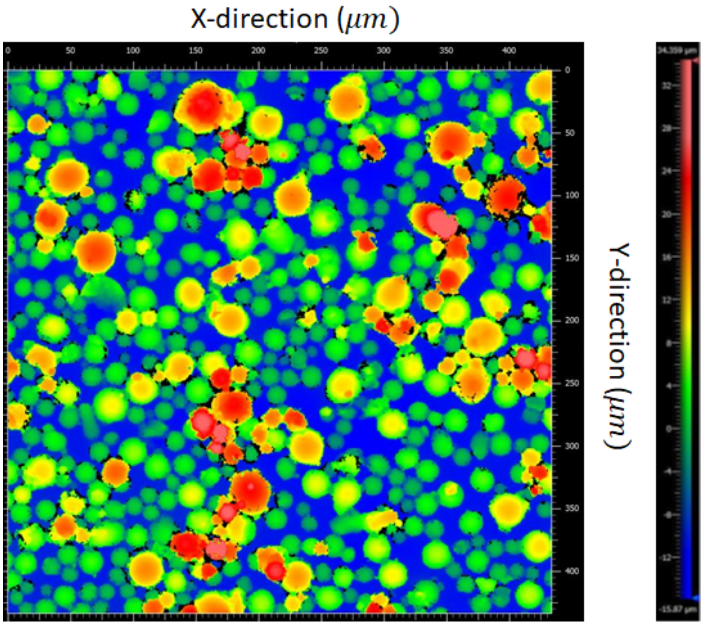

Figure 5. CSI image of one layer of Inconel 718 powder; the color bar indicates the depth/height profile of the particles relative to the bed (= −15.87 µm). The particles in green range in diameter from 10 to 15 µm, while the diameters of particles in yellow to orange range from 20 to 25 µm; the larger particles (in red) have diameters in the range of 40 to 45 µm. There are certain particles in the image shown in deep red that have comparable diameters to the particles in green, which is an indication of a smaller particle resting on top of other particles.

The image in Figure 5 shows a scanned area of 500 µm × 500 µm with the scan time equaling 5 min. The particles are color-coded ranging from green to red corresponding to different heights from the baseline value (= −15.87 µm). As evident from the Figure 5, majority of the imaged particles are spherical in shape and thus can be correlated to the respective particle diameters. Thus, using the depth profile, we were able to obtain the PSD in a straightforward manner and allowing for suitable comparisons with SEM images.

Having examined the PSD variation, we now turn our attention to examining the evolution in morphology of the particles as a function of build cycle. As discussed earlier, SEM images were used for determining the circularity of the particles, and any deviations in the extent of circularity is used as a measure of morphology change.

Circularity of the particles was also calculated using ImageJ based on Eq 1 [28] and was averaged over the examined particles for each build. The variation in circularity is given in Figure 6.

$$Circularity = \sqrt{4\pi \frac{area}{perimeter^2}} \tag{1}$$

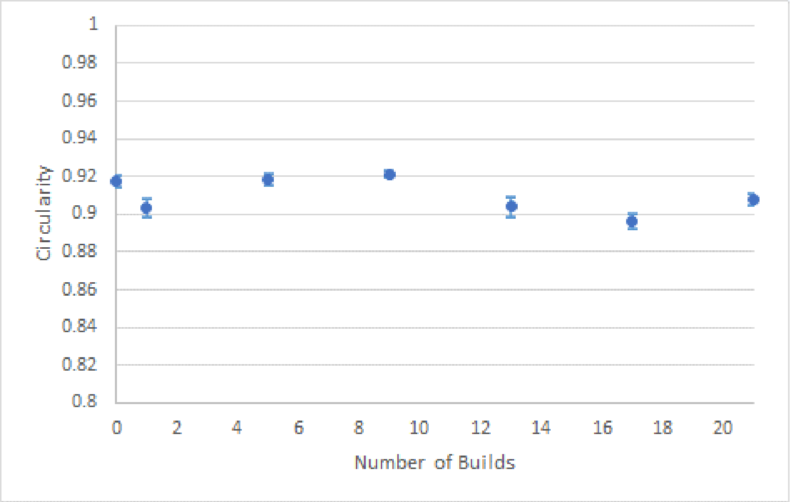

Figure 6. Variation in circularity as a function of build-cycle.

An interesting result that can gleaned from Figure 6 is the invariance in the average circularity as a function of cycle number, similar to the lack of systematic variation in the D50 values. This observation can be attributed to the fact that after every build cycle, the powders are sieved which leads to the removal of agglomerates, spatter, and satellited particles that are bigger than the preset value (53 µm) as discussed earlier.

To evaluate the possible changes in the chemistry of the powder as a function of build-cycles, EDS data for virgin, 9th, and 21st build-cycles are provided in Table 2. For brevity, we only provide data on these select samples. Reassuringly, the variations in the major constituents (listed in Table 2) are well within detection limits associated with EDS used in this work and thus we can conclude that there is no significant change in the chemical composition of the powder even after recycling. We also note that oxygen content was found to be below 1.0% for all samples, but due to potential limits associated with EDS in detecting oxygen, we have not reported the oxygen content in Table 2.

Table 2. EDS mass percent (%) of elements present at different build-cycles.

Element	Virgin	9 cycles	21 cycles
Nickel	42.63	41.93	44.44
Chromium	19.67	18.79	19.00
Iron	16.25	16.37	17.23
Carbon	7.17	7.65	5.83
Niobium	5.98	5.52	5.07
Molybdenum	2.88	2.69	2.62
Copper	1.67	1.88	1.76
Aluminum	0.82	1.04	0.66
Titanium	1.1	1.32	0.93
Cobalt	0.68	0.82	1.01
Manganese	0.11	0.09	0.18
Silicon	0.03	0.02	0.04

Finally, we examine the porosity and mechanical properties of the built-samples. We focus on three different samples, corresponding to build-cycle 1, 5, and 9. Table 3 provides the porosity and representative mechanical properties of the different samples. There is a slight variation in porosity, which follows the variation in the respective D50 trends. A typical optical micrograph that was used for measuring porosity is given in Figure 7. This variation is consistent with the trends in UTS and YS; i.e. (slightly) lower the porosity, (slightly) higher the UTS and YS. However, these variations are not significant enough to be considered important, and statistically are well within accepted ranges.

Table 3. Variation in porosity and mechanical properties of LBPF-fabricated samples as a function of build-cycle.

Cycle #	D50 (μm)	Percent area of porosity	Ultimate tensile strength (MPa)	Yield strength (MPa)
1	18.14	1.02	1325 ± 19	1069 ± 8
5	17.69	1.61	1340 ± 7	1116 ± 18
9	18.45	1.26	1332 ± 8	1095 ± 14

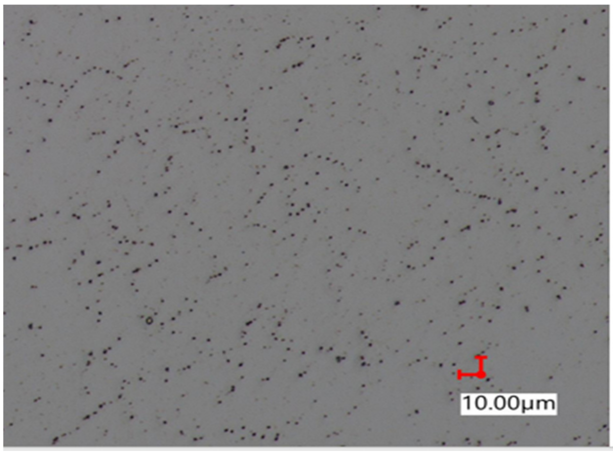

Figure 7. Optical micrograph of a polished cross-section of a printed part corresponding to build-cycle 5, which was used for porosity evaluation.

5. Conclusions

The characterization of particle size distribution (PSD) of Inconel 718 as a function of build cycle (21 cycles) showed no significant changes other than a very slight shift towards larger particles. In a similar fashion, changes in morphology and chemical compositions were insignificant too. The corresponding samples also show very similar porosity and mechanical behavior, though there seems to be slight variations that correlate to slight changes in the D50 value of the underlying PSD. These results clearly and unambiguously demonstrate that unused powder during a build can be reliably recycled for subsequent builds, without any compromise in powder characteristics, as long precautions such as sieving are undertaken.

While scanning electron microscopy (SEM) was the primary method for size, and morphology analysis, an alternate method namely coherent scanning interferometry (CSI) that was potentially faster, cheaper and easier to implement for imaging was examined with respect to SEM. Based on comparison in terms of estimating PSD, it was seen that CSI provides an equally good alternative to SEM, while having added advantages in terms of implementation.

Conflict of interest

All authors declare no conflicts of interest in this paper.

References

1. Wei C, Zhang Z, Cheng D, et al. (2020) An overview of laser-based multiple metallic material additive manufacturing: from macro-to micro-scales. *Int J Extreme Manuf* 3: 012003. https://doi.org/10.1088/2631-7990/abce04
2. Gu DD, Meiners W, Wissenbach K, et al. (2012) Laser additive manufacturing of metallic components: materials, processes and mechanisms. *Int Mater Rev* 57: 133–164. https://doi.org/10.1179/1743280411Y.0000000014
3. Hann BA (2016) Powder reuse and its effects on laser based powder fusion additive manufactured alloy 718. *SAE Int J Aerosp* 9: 209–214. https://doi.org/10.4271/2016-01-2071
4. Slotwinski JA, Garboczi EJ, Stutzman PE, et al. (2014) Characterization of metal powders used for additive manufacturing. *J Res Natl Inst Stan* 119: 460. https://doi.org/10.6028/jres.119.018
5. Cordova L, Campos M, Tinga T (2019) Revealing the effects of powder reuse for selective laser melting by powder characterization. *JOM* 71: 1062–1072. https://doi.org/10.1007/s11837-018-3305-2
6. Ardila LC, Garciandia F, González-Díaz JB, et al. (2014) Effect of IN718 recycled powder reuse on properties of parts manufactured by means of selective laser melting. *Phys Procedia* 56: 99–107. https://doi.org/10.1016/j.phpro.2014.08.152
7. Paccou E, Mokhtari M, Keller C, et al. (2021) Investigations of powder reusing on microstructure and mechanical properties of Inconel 718 obtained by additive manufacturing. *Mat Sci Eng A-Struct* 828: 142113. https://doi.org/10.1016/j.msea.2021.142113
8. Emminghaus N, Hoff C, Hermsdorf J, et al. (2021) Residual oxygen content and powder recycling: Effects on surface roughness and porosity of additively manufactured Ti-6Al-4V. *Addit Manuf* 46: 102093. https://doi.org/10.1016/j.addma.2021.102093
9. Soundarapandiyan G, Johnston C, Khan RHU, et al. (2021) The effects of powder reuse on the mechanical response of electron beam additively manufactured Ti6Al4V parts. *Addit Manuf* 46: 102101. https://doi.org/10.1016/j.addma.2021.102101
10. Moghimian P, Poirié T, Habibnejad-Korayem M, et al. (2021) Metal powders in additive manufacturing: A review on reusability and recyclability of common titanium, nickel and aluminum alloys. *Addit Manuf* 43: 102017. https://doi.org/10.1016/j.addma.2021.102017
11. Fiegl T, Franke M, Raza A, et al. (2021) Effect of AlSi10Mg0.4 long-term reused powder in PBF-LB/M on the mechanical properties. *Mater Design* 212: 110176. https://doi.org/10.1016/j.matdes.2021.110176

12. Gruber K, Smolina I, Kasprowicz M, et al. (2021) Evaluation of Inconel 718 metallic powder to optimize the reuse of powder and to improve the performance and sustainability of the laser powder bed fusion (LPBF) process. *Materials* 14: 1538. https://doi.org/10.3390/ma14061538
13. Paccou E, Mokhtari M, Keller C, et al. (2021) Investigations of powder reusing on microstructure and mechanical properties of Inconel 718 obtained by additive manufacturing. *Mat Sci Eng A-Struct* 828: 142113. https://doi.org/10.1016/j.msea.2021.142113
14. Sendino S, Martinez S, Lamikiz A (2020) Characterization of IN718 recycling powder and its effect on LPBF manufactured parts. *Procedia CIRP* 94: 227–232. https://doi.org/10.1016/j.procir.2020.09.043
15. Hilaire A, Andrieu E, Wu X (2019) High-temperature mechanical properties of alloy 718 produced by laser powder bed fusion with different processing parameters. *Addit Manuf* 26: 147–160. https://doi.org/10.1016/j.addma.2019.01.012
16. Martin JH, Yahata BD, Hundley JM, et al. (2017) 3D printing of high-strength aluminium alloys. *Nature* 549: 365–369. https://doi.org/10.1038/nature23894
17. Jankovics D, Gohari H, Tayefeh M, et al. (2018) Developing topology optimization with additive manufacturing constraints in ANSYS®. *IFAC-PapersOnLine* 51: 1359–1364. https://doi.org/10.1016/j.ifacol.2018.08.340
18. Brown CU, Brown CU, Jacob G, et al. (2018) The effects of laser powder bed fusion process parameters on material hardness and density for nickel alloy 625, *NIST Advanced Manufacturing Series*. https://doi.org/10.6028/NIST.AMS.100-19
19. Lane B, Mekhontsev S, Grantham S, et al. (2016) Design, developments, and results from the NIST additive manufacturing metrology testbed (AMMT). *Solid Freeform Fabrication 2016: Proceedings of the 26th Annual International Solid Freeform Fabrication Symposium—An Additive Manufacturing Conference*, 1145–1160.
20. Bennett JL, Kafka OL, Liao H, et al. (2018) Cooling rate effect on tensile strength of laser deposited Inconel 718. *Procedia Manuf* 26: 912–919. https://doi.org/10.1016/j.promfg.2018.07.118
21. Hebert RJ (2016) Metallurgical aspects of powder bed metal additive manufacturing. *J Mater Sci* 51: 1165–1175. https://doi.org/10.1007/s10853-015-9479-x
22. Savalani MM, Pizarro JM (2016) Effect of preheat and layer thickness on selective laser melting (SLM) of magnesium. *Rapid Prototyp J* 22: 115–122. https://doi.org/10.1108/RPJ-07-2013-0076
23. Averyanova M, Bertrand PH, Verquin B (2011) Studying the influence of initial powder characteristics on the properties of final parts manufactured by the selective laser melting technology. *Virtual Phys Prototyp* 6: 215–223. https://doi.org/10.1080/17452759.2011.594645
24. Gomez C, Su R, Thompson A, et al. (2017) Optimization of surface measurement for metal additive manufacturing using coherence scanning interferometry. *Opt Eng* 56: 111714. https://doi.org/10.1117/1.OE.56.11.111714
25. Townsend A, Senin N, Blunt L, et al. (2016) Surface texture metrology for metal additive manufacturing: a review. *Precis Eng* 46: 34–47. https://doi.org/10.1016/j.precisioneng.2016.06.001

26. DePond PJ, Guss G, Ly S, et al. (2018) In situ measurements of layer roughness during laser powder bed fusion additive manufacturing using low coherence scanning interferometry. *Mater Design* 154: 347–359. https://doi.org/10.1016/j.matdes.2018.05.050
27. Material Data Sheet EOS NickelAlloy IN718, Material Data Sheet Technical Data. EOS, 2022. Available from: https://www.eos.info/03_system-related-assets/material-related-contents/metal-materials-and-examples/metal-material-datasheet/nickelalloy-inconel/material_datasheet_eos_nickelalloy_in718_en.pdf.
28. Ferreira T, Rasband W (2012) ImageJ User Guide. Available from: https://imagej.nih.gov/ij/docs/guide/.